Downpour Dynamics: Outsized impacts of storm events on unprocessed atmospheric nitrate export in an urban watershed

Joel T. Bostic[1,2], David M. Nelson[1], Keith N. Eshleman[1]

[1]University of Maryland Center for Environmental Science, Appalachian Lab, Frostburg, Maryland, USA
[2]Garrett College, McHenry, MD, USA

Correspondence to: Joel Bostic (jbostic@umces.edu)

Abstract. Water-quality impacts of streamwater nitrate (NO_3^-) on downstream ecosystems are largely determined by the load of NO_3^- from the watershed to surface waters. The largest NO_3^- loads often occur during storm events, but it is unclear how loads of different NO_3^- sources change during storm events relative to baseflow or how watershed attributes might affect source export. To assess the role of stormflow and baseflow on NO_3^- source export and how these roles are modulated by hydrologic effects of land-use practices, we measured nitrogen ($\delta^{15}N$) and oxygen ($\Delta^{17}O$) isotopes of NO_3^- and oxygen isotopes ($\delta^{18}O$) of water in rainfall and streamwater samples from before, during, and after eight storm events across 14 months in two Chesapeake Bay watersheds of contrasting land-use. Storms had a disproportionately large influence on the export of unprocessed atmospheric NO_3^- ($NO_3^-{}_{Atm}$) and a disproportionately small influence on export of terrestrial NO_3^- ($NO_3^-{}_{Terr}$) relative to baseflow in the developed urban watershed. In contrast, baseflow and stormflow had similar influences on $NO_3^-{}_{Atm}$ and $NO_3^-{}_{Terr}$ export in the mixed agricultural/forested watershed. An equivalent relationship between $NO_3^-{}_{Atm}$ deposition on impervious surfaces and event $NO_3^-{}_{Atm}$ streamwater export in the urban watershed suggests that impervious surfaces that hydrologically connect runoff to channels likely facilitate export of $NO_3^-{}_{Atm}$ during rainfall events. Additionally, larger rainfall events were more effective in exporting $NO_3^-{}_{Atm}$ in the urban watershed, with increased rainfall depth resulting in a greater fraction of event $NO_3^-{}_{Atm}$ deposition exported. Considering both projected increases in precipitation amounts and intensity and urban/suburban sprawl in many regions of the world, best management practices that reduce hydrologic connectivity of impervious surfaces will likely help to mitigate the impact of storm events on $NO_3^-{}_{Atm}$ export from developed watersheds.

1 Introduction

Increasing streamwater nitrate (NO_3^-) export over the past century has negatively impacted many downstream ecosystems globally (Kemp et al., 2005; Camargo and Alonso, 2006; Steffen et al., 2015; Stevens, 2019). The severity of impacts to receiving waters is partially determined by the magnitude of NO_3^- loads (i.e., product of concentration and discharge; NRC, 2000). As such, riverine NO_3^- loads are greatest during periods of high discharge, which often follow large precipitation events, and can therefore have an outsized impact on annual streamwater NO_3^- loads (Vaughan et al., 2017; Kincaid et al., 2020). Sources of NO_3^- comprising storm event loads can be variable and associated with changing hydrologic flowpaths during precipitation events (Buda and DeWalle, 2009). Exported loads of individual NO_3^- sources (e.g., atmospheric NO_3^-) are less often quantified during storm events than routine baseflow samples, however (Divers et al., 2014; Sabo et al., 2016). Thus, it is not clear whether storm events have a disproportionate impact relative to non-storm (i.e., baseflow) conditions on different NO_3^- sources. The impact of storm events relative to baseflow on sources of streamwater NO_3^- is particularly relevant given the increases in precipitation amount and intensity projected to be associated with future climate change (Walsh et al., 2014).

Precipitation can affect the amount, as well as the source, of NO_3^- exported in surface waters via the surface-to-stream flow path. During storms, NO_3^- can be transported to streams by either overland or subsurface pathways. Overland flow is associated with NO_3^- sources deposited or present on the land surface, such as unprocessed atmospheric NO_3^- ($NO_3^-{}_{Atm}$; Rose et al., 2015a). Subsurface flow is associated with NO_3^- sources abundant in soils and groundwater, such as fertilizer, microbial, and/or sewage (Cook and Herczeg, 2012). Both hydrologic flowpaths (and the respective NO_3^- sources) can be affected by human land-use activities (Paul and Meyer, 2001; Barnes and Raymond, 2010; Jarvis, 2020). For example, previous studies report that developed watersheds export relatively more $NO_3^-{}_{Atm}$ than less developed watersheds, presumably due to hydrologic changes created by impervious surfaces (Buda and DeWalle, 2009; Burns et al., 2009; Kaushal et al., 2011; Bostic et al., 2021). However, evidence is lacking for (1) the mechanism generating increased $NO_3^-{}_{Atm}$ export in developed watersheds and (2) quantitative impacts of storm event loads relative to baseflow, both of which could be useful for mitigating the effects of storms on streamwater NO_3^- export.

The stable isotope compositions of NO_3^- and water (H_2O) are powerful tools for distinguishing NO_3^- sources and hydrologic flow paths, respectively. For example, the oxygen isotope values ($\Delta^{17}O$) of NO_3^- allow for quantification of atmospheric and terrestrial sources of NO_3^- in streamwater (Michalski et al., 2003), and $\delta^{15}N$ and $\delta^{18}O$ values of NO_3^- permit inferences into the relative contributions of terrestrially-sourced NO_3^- ($NO_3^-{}_{Terr}$), such as fertilizer or sewage N (Kendall et al., 2007). Additionally, $\delta^{18}O$ values of H_2O can be used to assess the importance of overland versus subsurface flow through partitioning of stream flow into pre-event and event contributions (Sklash et al., 1976; McGuire and McDonnell, 2007). Few studies have coupled these isotopic tracers (Buda and DeWalle, 2009), however, despite their suitability to assess the effect of storm events on both hydrologic flow paths and export of different NO_3^- sources. Such information could provide mechanistic evidence for the commonly reported relationship between developed watersheds and $NO_3^-{}_{Atm}$ export.

Here we address the following research questions: How do storm events affect the total amount and sources of NO_3^- exported in streams relative to baseflow? And, more specifically, what is the relationship between hydrologic and biogeochemical effects of land use and the export of unprocessed atmospheric $NO_3^-{}_{Atm}$ and terrestrial NO_3^- during storm events and baseflow? These questions were addressed in two Chesapeake Bay watersheds of contrasting land-use. A two-watershed study is inherently comparative, potentially limiting the inferences that can be made regarding land-use effects. However, given the contrasting land uses (i.e., predominantly developed compared to mixed forest/agriculture) in these watersheds, we believe that this study can adequately address our research questions while presenting a "proof of concept" for future studies. To address these research questions, we collected moderate-frequency (45 minute – 12 hour) streamwater samples before, during, and after eight rainfall events, bulk rainfall samples corresponding to these events, as well as monthly baseflow samples, in two catchments within the broader Chesapeake Bay watershed. We then used $\delta^{15}N$, $\delta^{18}O$, and $\Delta^{17}O$ of NO_3^- and $\delta^{18}O$ of H_2O to determine NO_3^- sources and hydrologic flowpaths, respectively. The Chesapeake Bay region is ideal for our study: it is one of the most ecologically and economically important estuaries in the world (NOAA, 1990) that has experienced recent improvements in ecosystem health associated with declining N loads (Chanat et al., 2016; Lefcheck et al., 2018; Zhang et al., 2018), but uncertainty surrounds continued water quality improvements in part due to the effects of projected increases in precipitation intensity across its diverse land-use watershed (Najjar et al., 2010).

2 Materials and Methods

2.1 Study watersheds and field methods

To assess NO_3^- export dynamics during storm events, streamwater and rainfall samples were collected synchronously during eight events from two watersheds with outlets in Maryland, USA – Gwynns Falls at Villa Nova (GWN) and Gunpowder Falls at Glencoe (GUN) (Figure 1) – from September 2018 – October 2019. These watersheds have similar geology (Piedmont physiographic province; Fenneman, 1946) and climate (humid sub-tropical; Kottek et al., 2006), but differing land-use (one predominantly developed and the other mixed forest and agriculture), impervious surface coverage (Figure S1) and area (Table 1). Events were targeted based on forecast precipitation amounts of at least 2.5 cm and the same events were sampled at each site. Automated samplers (Teledyne ISCO 3700 Portable Sampler, Lincoln, NE) were used to collect streamwater samples into pre-cleaned 1L bottles across each storm hydrograph, including pre-storm baseflow, rising limbs, and falling limbs for most events at intervals ranging from 45 minutes – 12 hours (Figure S2). A pre-event baseflow sample was not collected for the first storm, thus any figures or analyses that compare pre-event baseflow to event mean concentrations or event-water fractions have seven data points. Storm sample collection ceased when discharge fell to approximately 200% of pre-event baseflow. Bulk rainfall samples corresponding to each event were collected using 7.5 cm diameter funnels approximately 1 m above ground level connected to pre-cleaned 1 L Nalgene bottles, with pre-cleaned table tennis balls used to limit evaporation. Streamwater and rainfall samples were placed on ice for 12 – 36 hours after collection, then processed in the laboratory within 24 – 48 hours. Both study watersheds are gaged by the United States Geological Survey; 15-minute and mean daily discharge data were obtained using the dataRetrieval R package (DeCicco, 2018). Mean event rainfall depth for each watershed was obtained from PRISM Climate Group (PRISM, 2014) using the prism R package (Hart and Bell, 2015).

2.2 Lab Methods

Streamwater and rainfall samples for NO_3^- concentration and isotope analyses were filtered (0.45 μm) and frozen within 48 hours of collection. Aliquots for water isotope measurements were stored in completely filled (i.e., no headspace) 20 mL bottles at room temperature prior to analysis. NO_3^- and nitrite (NO_2^-) concentrations were measured using flow-injection colorimetric analysis (Lachat Quikchem 8000 FIA+).

The $\Delta^{17}O$, $\delta^{18}O$, and $\delta^{15}N$ values of stream and rainfall NO_3^- were measured using a Thermo Delta V+ isotope ratio mass spectrometer (Bremen, Germany) via the denitrifier method (Sigman et al., 2001; Casciotti et al., 2002) with thermal decomposition (at 800° C) of N_2O to N_2 and O_2 (Kaiser et al., 2007) at the Central Appalachians Stable Isotope Facility. NO_2^- is denitrified using this method as well, but NO_2^- concentrations in stream and rainfall samples were low relative to NO_3^- ($NO_2^-/(NO_2^- + NO_3^-)$ mean = 0.006, range = 0.00 – 0.027). Measured isotope ratios were normalized using international reference standards USGS 34 ($\delta^{17}O$ = -14.8 ‰, $\delta^{18}O$ = -27.9 ‰) and USGS 35 ($\delta^{17}O$ = 51.5 ‰, $\delta^{18}O$ = 57.5 ‰) for O isotopes (Böhlke et al., 2003) and USGS 32 ($\delta^{15}N$ = 180 ‰) and USGS 34 ($\delta^{15}N$ = -1.8 ‰) for N isotopes (IAEA, 1995). Reference standards were measured throughout sample analysis in equal concentrations to samples (ranging from 100 – 200 nmol depending on sample NO_3^- concentration). Analytical precision of $\Delta^{17}O$ ($\Delta^{17}O \approx \delta^{17}O - 0.52 \times \delta^{18}O$) was estimated as 0.5 ‰, $\delta^{18}O$ as 1.4 ‰, and $\delta^{15}N$ as 1.8 ‰ (1 σ) , based on repeated measurements (n ≅ 200) of reference standards USGS 32 and USGS 35 and a laboratory reference standard "Chile NO_3^-" (Duda Energy 1sn 1 lb. Sodium Nitrate Fertilizer 99+% Pure Chile Saltpeter from Amazon.com). Accuracy of $\Delta^{17}O$, $\delta^{18}O$, and $\delta^{15}N$ were tracked using repeated measurements of IAEA-N3 (n = 19, mean $\Delta^{17}O$ = -0.1 ‰, $\delta^{18}O$ = 24.3 ‰, $\delta^{15}N$ = 4.5 ‰) and closely agreed with published values (IAEA, 1995; Michalski et al., 2002; Böhlke et al., 2003). Each streamwater and rainfall sample was measured 3 – 6 times to reduce analytical uncertainty and the mean of each sample was used in all analyses. Standard error of the mean ranged from 0.1 – 0.6 ‰, 0.1 – 1.6 ‰, and 0.1 – 1.6 ‰ for replicate measurements of $\Delta^{17}O$, $\delta^{18}O$, and $\delta^{15}N$ respectively.

Oxygen ($\delta^{18}O_{-H2O}$) isotopes of rainfall and streamwater were measured using a Picarro L2130-i via cavity ring down spectroscopy at the University of Wyoming Stable Isotope Facility. Measured isotope ratios were normalized to VSMOW using internal laboratory standards that were calibrated to international standards. Precision based on repeated measurements of internal standards was 0.2 ‰.

2.3 Quantification of atmospheric NO_3^- deposition

Event $NO_3^-{}_{Atm}$ deposition was quantified using the measured rainfall NO_3^- concentration and mean rainfall depth (Lovett et al., 2000; Nelson et al., 2018; Huang et al., 2020):

$$NO_{3-Atm}^{-} Deposition\ (g\ N\ ha^{-1}) = \frac{Rainfall\ Volume\ (L) \times Rainfall\ NO_3^-\ (mg\ N\ L^{-1})}{Watershed\ Area\ (ha)} \times (1 \times 10^{-3}) \quad \text{(eq. 1)}$$

where rainfall volume is the product of rainfall depth and watershed area and 1×10^{-3} is a conversion factor. Event $NO_3^-{}_{Atm}$ deposition onto impervious surfaces was then calculated by multiplying $NO_3^-{}_{Atm}$ deposition by the percent of impervious surfaces.

2.4 Quantification of unprocessed atmospheric and terrestrial NO_3^- in streams

Concentrations of $NO_3^-{}_{Atm}$ were quantified using $\Delta^{17}O$ values of terrestrial and rainfall end-members and total NO_3^- concentrations:

$$f_{Atm} = \frac{(\Delta^{17}O_{Stream} - \Delta^{17}O_{Terr})}{(\Delta^{17}O_{Precip} - \Delta^{17}O_{Terr})} \quad \text{(eq. 2)}$$

$$NO_{3Atm}^{-}(mg\ N\ L^{-1}) = f_{Atm} \times NO_{3Total}^{-}(mg\ N\ L^{-1}) \quad \text{(eq. 3)}$$

$$NO_{3Terr}^{-}(mg\ N\ L^{-1}) = NO_{3Total}^{-}(mg\ N\ L^{-1}) - NO_{3Atm}^{-}(mg\ N\ L^{-1}) \quad \text{(eq. 4)}$$

where $\Delta^{17}O_{Stream} = \Delta^{17}O$ of streamwater samples during either baseflow or storm events, $\Delta^{17}O_{Precip} = \Delta^{17}O$ of rainfall for a given event, $\Delta^{17}O_{Terr} = \Delta^{17}O$ of terrestrially sourced NO_3^- which is ≅ 0 ‰, $NO_3^-{}_{Terr}$ = terrestrial NO_3^-, and $NO_3^-{}_{Total}$ = measured streamwater NO_3^- concentrations. Uncertainty in $NO_3^-{}_{Atm}$ was estimated by propagating analytical uncertainty from repeated measures of $\Delta^{17}O_{Stream}$ and $\Delta^{17}O_{Precip}$.

2.5 Quantification of event loads and mean concentrations and monthly loads

Event loads of $NO_3^-{}_{Total}$ and $NO_3^-{}_{Atm}$ were calculated as:

$$L_{NO_3^-} = \sum_{i=1}^{n} C_i \times V_i \times (1 \times 10^{-3}) \quad \text{(eq. 5)}$$

where L = load of either $NO_3^-{}_{Total}$, $NO_3^-{}_{Atm}$, or $NO_3^-{}_{Terr}$ in g per event, C_i = concentration of either $NO_3^-{}_{Total}$ or $NO_3^-{}_{Atm}$ in mg N L^{-1} for sample i, and V_i = volume of water exported corresponding to sample i in L, and 1×10^{-3} is a conversion factor (mg to g). Event yields (g N ha^{-1} $event^{-1}$) of $NO_3^-{}_{Total}$, $NO_3^-{}_{Atm}$, and $NO_3^-{}_{Terr}$ were calculated by normalizing loads by watershed area. To assess potential bias in $NO_3^-{}_{Atm}$ load quantification between our method (i.e., multiple samples collected during a storm event; eq. 5) and methods in which a single sample is collected, we multiplied the mean daily discharge by $NO_3^-{}_{Atm}$ concentrations of each individual grab sample collected during a particular event. We compared these estimated loads with the "true" load (calculated using eq. 5) and calculated bias as the difference between the "true" load and loads estimated using a single sample and daily average discharge. Because traditional methods commonly use mean daily discharge, we only investigated bias for two events that included samples collected over one full day. We also calculated the event fraction of unprocessed atmospheric NO_3^- (f_{Atm}) using $\Delta^{17}O$ (eq. 2) and $\delta^{18}O$ (substituting $\delta^{18}O$ for $\Delta^{17}O$ in eq. 2 and assuming that baseflow samples for a corresponding storm represent the terrestrial NO_3^- end-member $\delta^{18}O$ value).

Event mean concentrations (EMC) of $NO_3^-{}_{Total}$ and $NO_3^-{}_{Atm}$ and event mean values (EMV) of $\Delta^{17}O$, $\delta^{18}O$, and $\delta^{15}N$ were calculated as:

$$EMC, EMV = \frac{\sum_{i=1}^{n}(C_i \times V_i)}{\sum_{i=1}^{n} V_i} \qquad \text{(eq. 6)}$$

where EMC = event mean concentration in mg N L^{-1} (for $NO_3^-{}_{Total}$ and $NO_3^-{}_{Atm}$), EMV = event mean value in ‰ ($\Delta^{17}O$, $\delta^{18}O$, and $\delta^{15}N$), C_i = either concentration of $NO_3^-{}_{Total}$ or $NO_3^-{}_{Atm}$ (mg N L^{-1}) or value of $\Delta^{17}O$, $\delta^{18}O$, or $\delta^{15}N$ (‰) corresponding to sample i, and V_i = volume of water exported corresponding to sample i (L).

Monthly loads of $NO_3^-{}_{Total}$ were estimated using Weighted Regressions on Time, Discharge, and Season Kalman Filter (WRTDS-K; Zhang and Hirsch, 2019). Regressions were calibrated using the entire period of record for NO_3^- (excluding our storm samples) to generate coefficients representing a greater range of hydroclimatological conditions than was realized in 13 months. NO_3^- concentration data for the entire period of record were obtained from the Chesapeake Bay Program water quality database (Chesapeake Bay Program, 2021). Our storm samples were excluded to generate similar estimates of monthly and annual loads used by monitoring agencies (e.g., Maryland Department of

Natural Resources, US Environmental Protection Agency) in these watersheds. Monthly yields (g N ha^{-1}) were calculated by dividing monthly loads by watershed area and monthly flow-weighted concentrations (mg N L^{-1}) were calculated by dividing monthly loads by monthly discharge. Uncertainty of $NO_3^-{}_{Total}$ was estimated using block bootstrapping methods for WRTDS-K (Zhang and Hirsch, 2019) and was propagated through all analyses using $NO_3^-{}_{Total}$ loads and/or yields.

The fraction of rainfall NO_3^- exported on an event basis was calculated as:

$$Fraction\ of\ rainfall\ NO3^{-}\ exported = \frac{NO_{3-Atm}^{-} Yield\ (g\ N\ ha^{-1})}{NO_{3-Atm}^{-} Deposition\ (g\ N\ ha^{-1})} \quad \text{(eq. 7)}$$

where event $NO_3^-{}_{Atm}$ deposition was calculated using eq. 1 and event $NO_3^-{}_{Atm}$ yield was calculated using eq. 5.

2.6 Terrestrial δ18O and δ15N calculation

Streamwater storm samples of $\delta^{18}O$ and $\delta^{15}N$ were corrected to remove the influence of $NO_3^-{}_{Atm}$ (Dejwakh et al., 2012), which has higher $\delta^{18}O$ values and can have lower $\delta^{15}N$ values than terrestrial NO_3^- (Elliott et al., 2007; Kendall et al., 2007). This was done to more carefully infer how terrestrial sources of NO_3^- might change during storm events, and it uses the following equations:

$$\delta^{15}N_{Terr} = \frac{(\delta^{15}N_{Stream} - \delta^{15}N_{Atm} \times f_{Atm})}{f_{Terr}} \quad \text{(eq. 8)}$$

$$\delta^{18}O_{Terr} = \frac{(\delta^{18}O_{Stream} - \delta^{18}O_{Atm} \times f_{Atm})}{f_{Terr}}$$

(eq. 9)

where $\delta^{15}N/\delta^{18}O_{Stream}$ = measured $\delta^{15}N$ or $\delta^{18}O$ of streamwater storm samples, $\delta^{15}N/\delta^{18}O_{Atm}$ = rainfall $\delta^{15}N$ or $\delta^{18}O$ for a given event, f_{Atm} = fraction of $NO_3^-{}_{Atm}$, as calculated using eq. 2, and f_{Terr} = 1- f_{Atm}.

2.7 Hydrograph separation

Water isotopes were used to quantify the proportion of event and pre-event water during storm events at or near peak discharge. The direct routing, or translation of rainfall to streamwater during the same event, was quantified as the event-water fraction (i.e., rainfall), whereas water present in the catchment prior to the storm event was classified as the pre-event water fraction (i.e., baseflow) using the following equations (Sklash et al., 1976):

$$f_{Event\ Water} + f_{Pre-Event\ Water} = 1 \qquad \text{(eq. 9)}$$

$$f_{Event\ Water} = \frac{\delta^{18}O_{PeakQ} - \delta^{18}O_{Baseflow}}{\delta^{18}O_{Precipitation} - \delta^{18}O_{Baseflow}} \qquad \text{(eq. 10)}$$

where $\delta^{18}O_{PeakQ}$ = $\delta^{18}O_{H2O}$ at or near peak discharge during storm events, $\delta^{18}O_{Baseflow}$ = $\delta^{18}O_{H2O}$ of streamwater just prior to storm event and hydrograph rise, and $\delta^{18}O_{Rainfall}$ = $\delta^{18}O_{H2O}$ of bulk rainfall samples during a given storm event. Event and pre-event water runoff can be quantified using these equations by multiplying runoff during peak stormflow by fractions of event and pre-event water. Uncertainty was estimated using published methods to account for analytical uncertainty and separation, or lack thereof, of end-members (Genereux, 1998). It has been shown that some of the assumptions of isotope-based hydrograph separation may be violated in mesoscale catchments (e.g., spatiotemporally constant end-member values; Klaus and McDonnell, 2013), thus we estimate event-water fractions and runoff for peak discharge only and apply these data cautiously.

2.8 Framework for interpreting baseflow and stormflow contributions

The importance of storm events relative to baseflow in streamwater NO_3^- export can be evaluated using a fractional export plot (Figure 2). In this plot the y-axis shows the fraction of annual nitrate loads exported during a single event (f_{NO3}) and the x-axis shows the fraction of annual discharge exported during a single event (f_{Runoff}). For example, if NO_3^- concentrations remain constant with changing discharge during a storm, the data would fall on the 1:1 line because its load is perfectly explained by discharge and both storm events and baseflow have equal impact on loads (Figure 2). If NO_3^- concentrations decrease with increasing discharge during a storm, the data would plot below the 1:1 line. Watersheds with events consistently plotting below the 1:1 line indicate that baseflow, relative to storm events, has an outsized impact on riverine nitrate loads. If NO_3^- concentrations increase with increasing discharge, the data would plot above the 1:1 line. Watersheds with events consistently plotting above the 1:1 line indicate that storm events have an outsized impact on riverine NO_3^- loads. This framework can be expanded further by quantifying the (potential) disproportionate effect of storm events on streamwater constituent loads relative to water yields. Dividing f_{NO3} by f_{Runoff} provides a single value to quantify the level of disproportionality:

$$Disproportionality\ Factor\ (DF) = \frac{f_{NO3}}{f_{Runoff}} \qquad \text{(eq. 11)}$$

DF can be interpreted using Figure 2: a value falling on the 1:1 line would have $DF = 1$, a value below the 1:1 line would have a $DF < 1$, and a value above the 1:1 line would have $DF > 1$. For example, an event with $DF = 4$ indicates that a given storm exported 4× more NO_3^- than water whereas an event with $DF = 0.5$ indicates that a storm exported 2× less NO_3^- than water, after both have been normalized to annual amounts.

2.9 Statistical analyses

All statistical tests were performed in R (R Development Core Team, 2019). A Wilcoxon ranked-sum test was used to compare EMC and EMV of paired streamwater storm and baseflow samples. Due to the presence of outliers, Theil-Sen slopes (calculated using the *senth* function in R) were used to assess relationships between most continuous variables (Helsel et al., 2020). Least squares linear regression was used when outliers were absent. Confidence intervals (95%) and p-values of Theil-Sen slopes were computed using bootstrapping (10,000 replicates) to incorporate uncertainty in *DF* and event-water fractions.

3 Results

Rainfall depth and chemistry (NO_3^- concentrations and isotopes, H_2O isotopes) were similar between watersheds for sampled events ($p > 0.1$, Table S1). Rainfall depths ranged from 1.90 – 8.10 cm, which corresponds to a range of 24-hour precipitation depth return intervals of <1 year (1-year return interval ≈ 6.75 cm) up to 2-year (2-year return interval ≈ 8.3 cm) in this region (Bonnin et al., 2004). Streamwater NO_3^- concentrations ranged from 0.05 – 0.26 mg N L^{-1}, $\delta^{15}N$-NO_3^- from -8.7 – -1.4 ‰, $\delta^{18}O$-NO_3^- from 48.0 – 69.6 ‰, and $\Delta^{17}O$-NO_3^- from 13.6 – 24.9 ‰. Streamflow was slightly more variable in GWN during storm events (Table S2): event mean runoff and event maximum runoff were higher in GWN ($p < 0.05$ and $p < 0.01$ respectively), but event median runoff was not different between the watersheds ($p = 0.11$). Across all flow conditions, NO_3^- concentrations were lower at GWN (median = 0.78 mg N L^{-1}) than GUN (median = 2.60 mg N L^{-1}). Baseflow NO_3^- concentrations were higher than stormflow NO_3^- EMCs in both watersheds, but differences were more pronounced at GWN (baseflow median = 1.79 mg N L^{-1}, storm median = 0.66 mg N L^{-1}, $p < 0.05$) than GUN (baseflow median = 3.06 mg N L^{-1}, storm median = 2.55 mg N L^{-1}, $p < 0.05$, Figure 3 and Table S3).

At GWN, values of $\delta^{15}N$ were higher in baseflow (median $\delta^{15}N$ = 7.6 ‰) than stormflow (EMV median $\delta^{15}N$ = 5.0 ‰, respectively, $p < 0.05$), whereas values of $\delta^{18}O\text{-}NO_3^-$ were lower in baseflow (median $\delta^{18}O$ = 3.9 ‰) than stormflow (EMV median $\delta^{18}O$ = 7.4 ‰, $p < 0.05$). In contrast, values of $\delta^{15}N$- and $\delta^{18}O\text{-}NO_3^-$ did not differ between baseflow and stormflow at GUN (baseflow median $\delta^{15}N$ = 6.2 ‰, $\delta^{18}O$ = 3.3 ‰; stormflow EMV median $\delta^{15}N$ = 6.1 ‰, $\delta^{18}O$ = 3.0 ‰; Figure 3 and Table S3). Values of $\delta^{18}O\text{-}NO_3^-{}_{Terr}$ were higher during baseflow at both sites ($p < 0.05$, Figure 3), whereas $\delta^{15}N\text{-}NO_3^-{}_{Terr}$ was higher during baseflow at GWN only ($p < 0.05$, Figure 3). Similarly, $\Delta^{17}O$ of NO_3^- was not significantly different between baseflow (median = 0.4 ‰) and stormflow (EMV median = 0.5 ‰) at GUN, but was lower during baseflow (median = 0.7 ‰) than stormflow (EMV median = 2.0 ‰, $p < 0.05$, Figure 3 and Table S3) at GWN.

Concentrations of $NO_3^-{}_{Terr}$ were more temporally variable than $NO_3^-{}_{Atm}$. Concentrations of $NO_3^-{}_{Terr}$ showed similar patterns to $NO_3^-{}_{Total}$ at both watersheds: higher during baseflow than storm events (GWN baseflow median = 1.72 mg N L^{-1}, stormflow median = 0.59 mg N L^{-1}; $p < 0.001$, GUN baseflow median = 3.03 mg N L^{-1}, stormflow median = 2.50 mg N L^{-1}; $p < 0.005$, Figure S3). Both GWN and GUN had similar $NO_3^-{}_{Atm}$ concentrations between baseflow and storm events (GWN baseflow median = 0.05 mg N L^{-1}, stormflow median = 0.06 mg N L^{-1}, $p > 0.05$, GUN baseflow median = 0.04 mg N L^{-1}, stormflow median = 0.06 mg N L^{-1}, $p > 0.05$, Figure S3).

Similar to NO_3^- concentrations and isotopes, $\delta^{18}O\text{-}H_2O$ values exhibited greater variability between baseflow and peak streamflow in GWN than in GUN. From baseflow to approximately peak streamflow, $\delta^{18}O\text{-}H_2O$ shifted by an absolute average of 2.1 ‰ at GWN but only 0.6 ‰ at GUN (Table S2). These shifts correspond to an average event-water fraction at peak storm discharge of 0.75 ±0.13 at GWN and 0.27 ±0.23 at GUN (Table S2). Event-water fraction uncertainty was relatively large for several events due to small separation between $\delta^{18}O\text{-}H_2O$ end members. For example, rainfall and pre-event baseflow end members were separated by only 0.5 ‰ during the 7/22/19 event at GUN, resulting in uncertainty of event-water fractions exceeding 1 (Tables S1 and S2).

Storms events have an outsized impact, relative to baseflow, on $NO_3^-{}_{Atm}$ export at GWN, as indicated by *DF* > 1 for 7 of 8 sampled events (mean = 2.6 ±0.4; Figure 2). The opposite relationship was observed for $NO_3^-{}_{Terr}$ at GWN (*DF* ≤ 1 for all sampled events, mean = 0.5 ±0.1) indicating that baseflow has an outsized impact on $NO_3^-{}_{Terr}$ loads relative to storm events. Conversely, *DF* values at GUN were approximately 1 for both $NO_3^-{}_{Atm}$ (mean = 1.1 ±0.2) and $NO_3^-{}_{Terr}$ (mean = 1.0 ±0.1), indicating that neither baseflow nor stormflow disproportionately impacted stream NO_3^- loads (Figure 2). Event-water fractions were positively, though not significantly, related to *DF* of $NO_3^-{}_{Atm}$ ($\tau = 0.32$, $p = 0.09$) and negatively related to *DF* of $NO_3^-{}_{Terr}$ across both watersheds (Figure 4; $\tau = -0.32$, $p < 0.05$). In GWN, the total rainfall depth for a given event was positively correlated with the fraction of deposited NO_3^- that was exported in streamwater during the same event ($\tau = 0.74$, $p < 0.05$), but there was no relationship for GUN (Figure 5). Additionally, there was a 1:1 relationship between the event $NO_3^-{}_{Atm}$ deposition on impervious surfaces and the event $NO_3^-{}_{Atm}$ streamwater export at GWN ($r^2 = 0.55$, $p < 0.05$), but not at GUN (Figure 6). $NO_3^-{}_{Atm}$ load estimates using traditional methods (concentration from a single grab sample multiplied by mean daily discharge) were biased (range = -197 % – 123 %, median absolute value = 36 %) relative to $NO_3^-{}_{Atm}$ load estimates using the multiple samples we collected across the storm hydrograph for the two events that encompassed a full day.

4 Discussion

Hydrologic effects of impervious surfaces likely drive the disproportionate impact of storm events on $NO_3^-{}_{Atm}$, and of baseflow on $NO_3^-{}_{Terr}$, in the more developed watershed (GWN). Impervious surfaces increase peak storm runoff (Arnold and Gibbons, 1996; Walsh et al., 2005), but differences in peak discharge alone are not the sole explanation for the contrasting results of *DF* for $NO_3^-{}_{Terr}$ and $NO_3^-{}_{Atm}$ between the watersheds. Sampled events with overlapping f_{Runoff} between sites (i.e., similar x-axis values on Figure 2) indicate that the difference between f_{NO3} for $NO_3^-{}_{Terr}$ and $NO_3^-{}_{Atm}$ is much greater at the more developed (GWN) than the less developed watershed (GUN; i.e., different y-axis values on Figure 2). Thus, it is the overland routing of rainfall, and $NO_3^-{}_{Atm}$ dissolved therein, that likely contributes to the outsized impact of storm events on $NO_3^-{}_{Atm}$ in the developed watershed. Although both watersheds show a positive relationship between event-water fractions and *DF* of $NO_3^-{}_{Atm}$ (p =

0.09, Figure 4), event-water fractions are much greater in the more developed watershed, GWN (green triangles in Figure 4). Higher event-water fractions promote greater export of $NO_3^{-}{}_{Atm}$ by reducing the potential for biological processing or retention. Our results provide evidence (i.e., increased event-water fractions, proportional streamwater export of impervious $NO_3^{-}{}_{Atm}$ deposition) for the mechanism (i.e., direct routing of rainfall $NO_3^{-}{}_{Atm}$ to streams) that generates increased $NO_3^{-}{}_{Atm}$ export in more developed watersheds, which thus expands on previous research demonstrating that more developed watersheds export relatively more $NO_3^{-}{}_{Atm}$ (Buda and DeWalle, 2009; Burns et al., 2009; Kaushal et al., 2011; Bostic et al., 2021).

Our study collected samples across the storm hydrograph and measured $\Delta^{17}O$ of NO_3^{-}, which provided a more accurate load estimates of, and insights into, storm $NO_3^{-}{}_{Atm}$ export than $\delta^{18}O$ of NO_3^{-}. For example, estimates of daily $NO_3^{-}{}_{Atm}$ loads were biased by a median absolute value of 36% using standard methods (i.e., daily average discharge multiplied by $NO_3^{-}{}_{Atm}$ concentration, estimated using $\Delta^{17}O$, of a single grab sample; Tsunogai et al., 2014; Rose et al., 2015b; Nakagawa et al., 2018) when compared to "true" daily loads calculated using samples collected across the storm hydrograph from two events that encompassed a full day. Additionally, use of $\Delta^{17}O$ generally provides more certain estimates of $NO_3^{-}{}_{Atm}$ fractions and concentrations than $\delta^{18}O$ because biological processing (e.g., assimilation, denitrification) can change the $\delta^{18}O$ of NO_3^{-} and generate large uncertainty (± ~30‰, Kendall et al., 2007) in the $\delta^{18}O$-$NO_3^{-}{}_{Terr}$ end-member and ultimately estimates of $NO_3^{-}{}_{Atm}$ (Tsunogai et al., 2016). $\Delta^{17}O$ of NO_3^{-}, due to its mass-independent fractionation origin, is not subject to the same variability associated with biological processing as $\delta^{18}O$, thereby decreasing uncertainty in $NO_3^{-}{}_{Atm}$ estimates (Young et al., 2002; Michalski et al., 2004; Kendall et al., 2007). Indeed, average event $NO_3^{-}{}_{Atm}$ fractions (i.e., $\frac{NO_{3Atm}^{-}}{NO_{3Total}^{-}}$) would have been underestimated by an average of 3% (range = 0 – 7 %) at both sites if using $\delta^{18}O$-NO_3^{-} only (Figure S4), but with a greater effect at the more developed site (GWN). An average underestimate of 3% may appear minor, but it is notable considering that event $NO_3^{-}{}_{Atm}$ fractions averaged 2% and 10% in the less and more developed watersheds, respectively. Increased accuracy of $NO_3^{-}{}_{Atm}$ export during storm events combined with the *DF* conceptual framework (Figure 2) provides a relatively simple means of assessing whether storm events or baseflow have an outsized impact on NO_3^- source export. More accurate estimates of $NO_3^-{}_{Atm}$ export also allow for more quantitative investigations into the role of impervious surfaces in routing event rainfall $NO_3^-{}_{Atm}$ to streams.

Impervious areas in the developed watershed are effective conduits of $NO_3^-{}_{Atm}$ to surface waters, as demonstrated by the approximately proportional relationship between event streamwater $NO_3^-{}_{Atm}$ export and event $NO_3^-{}_{Atm}$ deposition on impervious surfaces (Figure 6). This relationship provides evidence, in addition to higher event-water fractions (Figure 4), for the mechanism of impervious surfaces enhancing export of $NO_3^-{}_{Atm}$ during storm events. The 1:1 correspondence of this relationship is surprising, however. For 100% of rainfall $NO_3^-{}_{Atm}$ on impervious surfaces to be exported as streamwater during a given event (i.e., 1:1 relationship), all impervious area in the watershed would have to be hydrologically connected to surface waters (i.e., effective impervious areas; Shuster et al., 2005). In a mesoscale (84 km^2) and heterogeneous watershed such as GWN, the total impervious area is not equivalent to effective impervious area. Rather, many impervious surfaces drain onto pervious surfaces, or are "ineffective" at directly routing precipitation to channels (Walesh, 1989; but we note that certain pervious surfaces, such as reclaimed mine lands, effectively function as impervious, e.g., Negley and Eshleman 2006). It is likely that the observed 1:1 relationship (Figure 6) is additionally affected by flushing of dry $NO_3^-{}_{Atm}$ deposition from effective impervious areas. Dry NO_3^- deposition, similar to wet deposition, inherits positive $\Delta^{17}O$ values (~15 – 30 ‰; Nelson et al., 2018) and is generally higher in urban relative to rural areas both locally (Lovett et al., 2000; Bettez and Groffman, 2013) and globally (Decina et al., 2019). Thus, flushing of dry NO_3^- deposition residing on impervious surfaces (or on surfaces such as leaves that can wash onto impervious surfaces) during storm events could contribute to the 1:1 relationship observed in the more developed watershed (green circles in Figure 6).

$\Delta^{17}O$ of NO_3^- can additionally be used to "correct" $\delta^{15}N$ and $\delta^{18}O$ values (eqs. 7 and 8) to better indicate isotope values of terrestrial NO_3^- sources (Dejwakh et al., 2012). Values of both $\delta^{15}N_{Terr}$ and $\delta^{18}O\text{-}NO_3^-{}_{Terr}$ during storm events fall within the range of values that are typical of natural "soil" and fertilizer (Kendall et al., 2007), but interestingly, $NO_3^-{}_{Terr}$ isotope values decreased during storm events relative to baseflow in both watersheds (though not significantly for $\delta^{15}N$ in GUN; Figure 3). This shift to lower $\delta^{15}N_{Terr}$ and $\delta^{18}O\text{-}NO_3^-{}_{Terr}$ values during storm events may reflect the flushing of less "processed" NO_3^- sources from upper soil horizons (Creed et al., 1996), as processing (e.g., denitrification) generally leaves the remaining NO_3^- with more positive $\delta^{15}N$ and $\delta^{18}O$ values due to biologically-mediated fractionation (Denk et al., 2017). Lower $\delta^{15}N_{Terr}$ during storm events relative to baseflow was not statistically significant in the mixed agricultural/forested watershed (GUN), but this was due to a single event in which $\delta^{15}N_{Terr}$ increased from baseflow to stormflow. Impervious surfaces in the developed watershed likely reduce flushing of this lower $\delta^{18}O$-$NO_3^-{}_{Terr}$ by restricting infiltration, but 30% of this watershed is not "developed" (and a higher percentage contains pervious surfaces), which likely contributes to the similarity in $NO_3^-{}_{Terr}$ isotope patterns between study watersheds. Additionally, relatively lower $NO_3^-{}_{Terr}$ isotope values in storm events could be due to reduced in-stream NO_3^- uptake (e.g., assimilation, denitrification) during periods of elevated discharge (Grimm et al., 2005). Biological NO_3^- uptake generally fractionates against heavier isotopes which increases isotope ratios of the remaining NO_3^- (Kendall et al., 2007). If in-stream NO_3^- uptake rates are reduced during high flows, the resulting effect could contribute to the lower $NO_3^-{}_{Terr}$ isotope values during storm events. Relatively lower $\delta^{18}O$- $NO_3^-{}_{Terr}$ values during storm events relative to baseflow, and associated insights into watershed-scale N biogeochemistry, were only realized by using $\Delta^{17}O$ to "correct" $\delta^{18}O$ values. Without this correction, $\delta^{18}O$-NO_3^- during storm events is strongly influenced by elevated $\delta^{18}O$ of $NO_3^-{}_{Atm}$, as shown by the similar patterns between $\Delta^{17}O$ and "uncorrected" $\delta^{18}O$ in the more developed watershed (Figure 3).

Large inputs and stores of N associated with agricultural activity likely contribute to baseflow and storm events having similar impacts on $NO_3^-{}_{Terr}$ and $NO_3^-{}_{Atm}$ export in the mixed agricultural/forested watershed (GUN). *DF*s of both $NO_3^-{}_{Terr}$ and $NO_3^-{}_{Atm}$ were approximately 1, indicating that loads are primarily explained by changes in discharge. Nutrients, including NO_3^-, showing similar patterns (loads explained primarily by discharge) over annual time-scales have been attributed to large stores of NO_3^- associated with agricultural inputs (Basu et al., 2010; Thompson et al., 2011). With significant agricultural land-use, both currently (41.3% in 2016; Table 1) and historically (~58% in 1960; O'Bryan and McAvoy, 1966), and consistently high NO_3^- concentrations in streamwater, GUN likely has large stores of NO_3^- in soil and groundwater. Interestingly, our results demonstrate the control of discharge on $NO_3^-{}_{Terr}$ and $NO_3^-{}_{Atm}$ loads over storm-event time scales, suggesting that large reservoirs of NO_3^- contribute to streamwater export of nutrients across varied flow conditions and not just baseflow.

The combination of our results with projections of increasing frequency of intense precipitation events (Najjar et al., 2010; Walsh et al., 2014) and increasing urban and suburban sprawl (Jantz et al., 2005; Seto et al., 2012) suggest that $NO_3^-{}_{Atm}$ may become a relatively more important NO_3^- source to downstream waters, assuming no change in NO_3^- deposition rates. This assumption may not be valid everywhere, however; for example, NO_3^- deposition is declining locally (i.e., mid-Atlantic USA; Li et al., 2016) but increasing across many regions (i.e., east Asia; Liu et al., 2013). In our more developed watershed, the positive correlation between rainfall and the fraction of deposited NO_3^- exported in streamwater (Figure 5) suggests that large storm events may export proportionally greater fractions of rainfall $NO_3^-{}_{Atm}$ in urbanizing catchments and increased loads of $NO_3^-{}_{Atm}$ to downstream waters. Best management practices in developed watersheds (e.g., stormwater control measures) can mitigate these potential impacts by increasing infiltration of rainfall (and NO_3^- dissolved in rainfall) and reducing hydrologic connectivity of overland flowpaths (i.e., decrease effective impervious areas; Lee and Heaney, 2003; Walsh et al., 2009), both of which may reduce the load of $NO_3^-{}_{Atm}$ and the proportion of "event" water in streams during storm events. Such practices may additionally reduce $NO_3^-{}_{Terr}$ loads by stimulating denitrification (Bettez and Groffman, 2012), but could also increase the importance of baseflow in NO_3^- export due to increased infiltration. Thus, monitoring of both baseflow and storm events is necessary to quantify potential changes and make targeted water-quality management decisions. Finally, best management practices intended to reduce $NO_3^-{}_{Atm}$ loads in developed watersheds via increased infiltration may provide numerous co-benefits, including reduced runoff (Hood et al., 2007) and higher baseflow (Fletcher et al., 2013), both of which could help restore aquatic ecosystems impacted by urbanization (Walsh et al., 2005).

5. Conclusion

We found that stormflow has a disproportionately large impact on $NO_3^-{}_{Atm}$ export whereas baseflow has a disproportionately small impact on $NO_3^-{}_{Terr}$ export in a moderately developed watershed. In contrast, neither stormflow nor baseflow have an outsized impact on $NO_3^-{}_{Atm}$ or $NO_3^-{}_{Terr}$ export in a mixed land-use watershed with significant agriculture. Hydrologic connectivity of overland flow paths associated with impervious surfaces likely promote rapid transport of $NO_3^-{}_{Atm}$ to streams during storm events in the more developed watershed, with higher rainfall storms exporting a greater fraction of deposited NO_3^- than lower rainfall events and event $NO_3^-{}_{Atm}$ streamwater export approximately equaling rainfall $NO_3^-{}_{Atm}$ on impervious surfaces. Large reserves of new and/or legacy agricultural-associated nitrogen in soils in the mixed land-use watershed likely influenced the similar response of $NO_3^-{}_{Atm}$ or $NO_3^-{}_{Terr}$ to stormflow and baseflow.

Appendices

Not applicable.

Code availability

Not applicable.

Data availability

Complete data is presented in Tables S4 and S5.

Author contributions

DMN and KNE: Conceptualization, Methodology, Writing – Review and Editing, Supervision, Funding Acquisition

JTB: Conceptualization, Methodology, Investigation, Formal Analysis, Writing – Original Draft, Writing – Review and Editing, Visualization, Funding Acquisition

Acknowledgements

Thanks to Pavithra Pitumpe Arachchige and Jim Garlitz for NO_3^- concentration analysis. Robert Hirsch of the U.S. Geological Survey provided guidance on WRTDS-K and R scripts for estimating $NO_{3\text{-Total}}$ uncertainty. DMN, KNE, and JTB received support from Maryland Sea Grant under award NA14OAR4170090 R/WS-3 from the National Oceanic and Atmospheric Administration, U.S. Department of Commerce. JTB received support from Maryland Sea Grant under award SA75281900-A from the National Oceanic and Atmospheric Administration, U.S. Department of Commerce. This material is based upon work supported by the National Science Foundation Graduate Research Fellowship (to JTB) under Grant No. 1840380. Any opinion, findings, conclusions, recommendations expressed in this material are those of the authors and do not necessarily reflect the views of the National Science Foundation.

References

Arnold CL, Gibbons CJ. 1996. Impervious surface coverage: The emergence of a key environmental indicator. Journal of the American Planning Association 62: 243-258. https://doi.org/10.1080/01944369608975688

Barnes RT, Raymond PA. 2010. Land-use controls on sources and processing of nitrate in small watersheds: Insights from dual isotopic analysis. Ecological Applications 20: 1961-1978. https://doi.org/10.1890/08-1328.1

Basu NB, Destouni G, Jawitz JW, Thompson SE, Loukinova NV, Darracq A, Zanardo S, Yaeger M, Sivapalan M, Rinaldo A, Rao PSC. 2010. Nutrient loads exported from managed catchments reveal emergent biogeochemical stationarity. Geophysical Research Letters 37. https://doi.org/10.1029/2010GL045168

Bettez N, Groffman P. 2012. Denitrification potential in stormwater control structures and natural riparian zones in an urban landscape. Environmental Science & Technology 46 20: 10909-10917. https://doi.org/10.1021/es301409z

Bettez ND, Groffman PM. 2013. Nitrogen deposition in and near an urban ecosystem. Environmental Science & Technology 47: 6047-6051. https://doi.org/10.1021/es400664b

Böhlke JK, Mroczkowski SJ, Coplen TB. 2003. Oxygen isotopes in nitrate: New reference materials for ^{18}O:^{17}O:^{16}O measurements and observations on nitrate-water equilibration. Rapid Communications in Mass Spectrometry 17: 1835-1846. https://doi.org/10.1002/rcm.1123

Bonnin GM, Martin D, Lin B, Parzybok T, Yekta M, Riley D. 2004. Precipitation-frequency atlas of the United States. Volume 2 version 3.0. Delaware, District of Columbia, Illinois, Indiana, Kentucky, Maryland, New Jersey, North Carolina, Ohio, Pennsylvania, South Carolina, Tennessee, Virginia, West Virginia.

Bostic JT, Nelson DM, Sabo RD, Eshleman KN. 2021. Terrestrial nitrogen inputs affect the export of unprocessed atmospheric nitrate to surface waters: Insights from triple oxygen isotopes of nitrate. Ecosystems. https://doi.org/10.1007/s10021-021-00722-9

Buda AR, DeWalle DR. 2009. Dynamics of stream nitrate sources and flow pathways during stormflows on urban, forest and agricultural watersheds in central Pennsylvania, USA. Hydrological Processes 23: 3292-3305. https://doi.org/10.1002/hyp.7423

Burns DA, Boyer EW, Elliott EM, Kendall C. 2009. Sources and transformations of nitrate from streams draining varying land uses: Evidence from dual isotope analysis. Journal of Environmental Quality 38: 1149-1159. 10.2134/jeq2008.0371

Camargo JA, Alonso Á. 2006. Ecological and toxicological effects of inorganic nitrogen pollution in aquatic ecosystems: A global assessment. Environment International 32: 831-849. https://doi.org/10.1016/j.envint.2006.05.002

Casciotti KL, Sigman DM, Hastings MG, Böhlke J, Hilkert A. 2002. Measurement of the oxygen isotopic composition of nitrate in seawater and freshwater using the denitrifier method. Analytical Chemistry 74: 4905-4912. https://doi.org/10.1021/ac020113w

Chesapeake Bay Program. 2019. Chesapeake assessment and scenario tool (CAST). Chesapeake Bay Program Office.
Chesepeake Bay Program. 2021. Chesapeake Bay Program Water Quality Database, 1984-present. Accessed March 1, 2021 from http://www.chesapeakebay.net/data/downloads/cbp_water_quality_database_1984_present.

Chanat JG, Moyer DL, Blomquist JD, Hyer KE, Langland MJ. 2016. Application of a weighted regression model for reporting nutrient and sediment concentrations, fluxes, and trends in concentration and flux for the Chesapeake Bay nontidal water-quality monitoring network, results through water year 2012. Scientific Investigations Report. Reston, VA, p88. https://doi.org/10.3133/sir20155133
Cook PG, Herczeg AL. 2012. Environmental tracers in subsurface hydrology: Springer Science & Business Media. https://doi.org/10.1007/978-1-4615-4557-6

Creed IF, Band LE, Foster NW, Morrison IK, Nicolson JA, Semkin RS, Jeffries DS. 1996. Regulation of nitrate-N release from temperate forests: A test of the N flushing hypothesis. Water Resources Research 32: 3337-3354. https://doi.org/10.1029/96WR02399

DeCicco LA, Lorenz, D., Hirsch, R.M. 2018. dataRetrieval: R packages for discovering and retrieving water data available from U.S. Federal hydrologic web services. United States Geological Survey. 10.5066/P9X4L3GE

Decina SM, Hutyra LR, Templer PH. 2019. Hotspots of nitrogen deposition in the world's urban areas: A global data synthesis. Frontiers in Ecology and the Environment 18: 92-100. https://doi.org/10.1002/fee.2143

Dejwakh NR, Meixner T, Michalski G, McIntosh J. 2012. Using 17O to investigate nitrate sources and sinks in a semi-arid groundwater system. Environmental Science & Technology 46: 745-751. https://doi.org/10.1021/es203450z

Denk TRA, Mohn J, Decock C, Lewicka-Szczebak D, Harris E, Butterbach-Bahl K, Kiese R, Wolf B. 2017. The nitrogen cycle: A review of isotope effects and isotope modeling approaches. Soil Biology and Biochemistry 105: 121-137. https://doi.org/10.1016/j.soilbio.2016.11.015

Dingman SL. 1994. Physical hydrology. xii, 643 pp.

Divers, MT, Elliott, EM, Bain, DJ. Quantification of nitrate sources to an urban stream using dual nitrate isotopes. Environmental Science & Technology, 48: 10580-10587. https://doi.org/10.1021/es404880j

Edmund M. Hart and Kendon Bell. 2015. PRISM: Download data from the Oregon PRISM project.

Elliott EM, Kendall C, Wankel SD, Burns DA, Boyer EW, Harlin K, Bain DJ, Butler TJ. 2007. Nitrogen isotopes as indicators of NO_x source contributions to atmospheric nitrate deposition across the midwestern and northeastern United States. Environmental Science & Technology 41: 7661-7667. https://doi.org/10.1021/es070898t

Fenneman NM, Johnson, D.W. 1946. Physiographic divisions of the conterminus U.S. U.S. Geological Survey. Reston, VA.

Fletcher, T., Andrieu, H., Hamel, P. 2013. Understanding, management and modelling of urban hydrology and its consequences for receiving waters: A state of the art. Advances in Water Resources 51: 261-279. https://doi.org/10.1016/j.advwatres.2012.09.001

Genereux D. 1998. Quantifying uncertainty in tracer-based hydrograph separations. Water Resources Research 34: 915-919. https://doi.org/10.1029/98WR00010

Grimm NB, Sheibley RW, Crenshaw CL, Dahm CN, Roach WJ, Zeglin LH. N retention and transformation in urban streams. 2005. Journal of the North American Benthological Society 24(3): 626-642. https://doi.org/10.1899/04-027.1

Huang S, Wang F, Elliott EM, Zhu F, Zhu W, Koba K, Yu Z, Hobbie EA, Michalski G, Kang R, Wang A, Zhu J, Fu S, Fang Y. 2020. Multiyear measurements on $\Delta^{17}O$ of stream nitrate indicate high nitrate production in a temperate forest. Environmental Science & Technology 54: 4231-4239. https://doi.org/10.1021/acs.est.9b07839

Helsel DR, Hirsch RM, Ryberg KR, Archfield SA, Gilroy EJ. 2020. Statistical methods in water resources. Techniques and Methods. Reston, VA, p. 484. https://doi.org/10.3133/tm4A3

Homer C, Dewitz J, Jin S, Xian G, Costello C, Danielson P, Gass L, Funk M, Wickham J, Stehman S, Auch R, Riitters K. 2020. Conterminous united states land cover change patterns 2001–2016 from the 2016 national land cover database. ISPRS Journal of Photogrammetry and Remote Sensing 162: 184-199. https://doi.org/10.1016/j.isprsjprs.2020.02.019

Hood, M., Clausen, J., Warner, G. 2007. Comparision of stormwater lag times for low impact and traditional residential development. Journal of the American Water Resources Association 43: 1036-1046. https://doi.org/10.1111/j.1752-1688.2007.00085.x

IAEA. 1995. Reference and intercomparison materials for stable isotopes of light elements. Vienna: International Atomic Energy Agency.

Jantz P, Goetz S, Jantz C. 2005. Urbanization and the loss of resource lands in the Chesapeake Bay watershed. Environmental Management 36: 808-825. https://doi.org/10.1007

Jarvis NJ. 2020. A review of non-equilibrium water flow and solute transport in soil macropores: Principles, controlling factors and consequences for water quality. European Journal of Soil Science 71: 279-302. https://doi.org/10.1111/j.1365-2389.2007.00915.x

Kaiser J, Hastings MG, Houlton BZ, Röckmann T, Sigman DM. 2007. Triple oxygen isotope analysis of nitrate using the denitrifier method and thermal decomposition of N_2O. Analytical Chemistry 79: 599-607. https://doi.org/10.1021/ac061022s

Kaushal SS, Groffman PM, Band LE, Elliott EM, Shields CA, Kendall C. 2011. Tracking nonpoint source nitrogen pollution in human-impacted watersheds. Environmental Science & Technology 45: 8225-8232. https://doi.org/10.1021/es200779e

Kemp WM, Boynton WR, Adolf JE, Boesch DF, Boicourt WC, Brush G, Cornwell JC, Fisher TR, Glibert PM, Hagy JD. 2005. Eutrophication of Chesapeake Bay: Historical trends and ecological interactions. Marine Ecology Progress Series 303: 1-29. https://doi.org/10.3354/meps303001

Kendall C, Elliott, E, Wankel, S. 2007. Tracing anthropogenic inputs of nitrogen to ecosystems: Blackwell Publishing. https://doi.org/10.1002/9780470691854.ch12

Kincaid DW, Seybold EC, Adair EC, Bowden WB, Perdrial JN, Vaughan MCH, Schroth AW. 2020. Land use and season influence event-scale nitrate and soluble reactive phosphorus exports and export stoichiometry from headwater catchments. Water Resources Research 56. https://doi.org/10.1029/2020WR027361

Klaus J, McDonnell J. 2013. Hydrograph separation using stable isotopes: Review and evaluation. Journal of Hydrology 505: 47-64. https://doi.org/10.1016/j.jhydrol.2013.09.006

Kottek M, Grieser J, Beck C, Rudolf B, Rubel F. 2006. World map of the Köppen-Geiger climate classification updated. Meteorologische Zeitschrift 15: 259-263. https://doi.org/10.1127/0941-2948/2006/0130.

Lee JG, Heaney JP. 2003. Estimation of urban imperviousness and its impacts on storm water systems. Journal of Water Resources Planning and Management 129: 419-426. https://doi.org/10.1061/(ASCE)0733-9496(2003)129:5(419)

Lefcheck JS, Orth RJ, Dennison WC, Wilcox DJ, Murphy RR, Keisman J, Gurbisz C, Hannam M, Landry JB, Moore KA. 2018. Long-term nutrient reductions lead to the unprecedented recovery of a temperate coastal region. Proceedings of the National Academy of Sciences 115: 3658-3662. https://doi.org/10.1073/pnas.1715798115

Li Y, Schichtel BA, Walker JT, Schwede DB, Chen X, Lehmann CM, Puchalski MA, Gay DA, Collett JL. 2016. Increasing importance of deposition of reduced nitrogen in the United States. Proceedings of the National Academy of Sciences 113: 5874-5879. https://doi.org/10.1073/pnas.1525736113

Liu, X., Zhang, Y., Wenxuan, H., Tang, A., Shen, J., Cui, Z., Vitousek, P., Erisman, J., Goudling, K., Christie, P., Fangmeier, A., Zhang, F. 2013. Enchanced nitrogen deposition over China. Nature 494: 459-462. https://doi.org/10.1038/nature11917

Lovett GM, Traynor MM, Pouyat RV, Carreiro MM, Zhu W-X, Baxter JW. 2000. Atmospheric deposition to oak forests along an urban–rural gradient. Environmental Science & Technology 34: 4294-4300. https://doi.org/10.1021/es001077q

McGuire K, McDonnell J. 2007. Stable isotope tracers in watershed hydrology. Stable isotopes in ecology and environmental science, p334-374. https://doi.org/10.1002/9780470691854.ch11

Michalski G, Meixner T, Fenn M, Hernandez L, Sirulnik A, Allen E, Thiemens M. 2004. Tracing atmospheric nitrate deposition in a complex semiarid ecosystem using Δ^{17}O. Environmental Science & Technology 38: 2175-2181. https://doi.org/10.1021/es034980+

Michalski G, Savarino J, Böhlke JK, Thiemens M. 2002. Determination of the total oxygen isotopic composition of nitrate and the calibration of a Δ^{17}O nitrate reference material. Analytical Chemistry 74: 4989-4993. https://doi.org/10.1021/ac0256282

Michalski G, Scott Z, Kabiling M, Thiemens MH. 2003. First measurements and modeling of Δ^{17}O in atmospheric nitrate. Geophysical Research Letters 30. https://doi.org/10.1029/2003GL017015

Najjar RG, Pyke CR, Adams MB, Breitburg D, Hershner C, Kemp M, Howarth R, Mulholland MR, Paolisso M, Secor D, Sellner K, Wardrop D, Wood R. 2010. Potential climate-change impacts on the Chesapeake Bay. Estuarine, Coastal and Shelf Science 86: 1-20. https://doi.org/10.1016/j.ecss.2009.09.026

Nakagawa F, Tsunogai U, Obata Y, Ando K, Yamashita N, Saito T, Uchiyama S, Morohashi M, Sase H. 2018. Export flux of unprocessed atmospheric nitrate from temperate forested catchments: A possible new index for nitrogen saturation. Biogeosciences 15: 7025-7042. https://doi.org/10.5194/bg-15-7025-2018

Negley, T.L. and Eshleman, K.N. 2006. Comparison of stormflow responses of surface-mined and forested watersheds in the Appalachian Mountains, USA. Hydrological Processes 20: 3467-3483. https://doi.org/10.1002/hyp.6148

Nelson DM, Tsunogai U, Ding D, Ohyama T, Komatsu DD, Nakagawa F, Noguchi I, Yamaguchi T. 2018. Triple oxygen isotopes indicate urbanization affects sources of nitrate in wet and dry atmospheric deposition. Atmospheric Chemistry and Physics 18: 6381-6392. https://doi.org/10.5194/acp-18-6381-2018

NRC. 2000. Clean coastal waters: Understanding and reducing the effects of nutrient pollution. Washington, DC: The National Academies Press. 428p. https://doi.org/10.17226/9812

O'Bryan, D., and McAvoy, R.L. 1966. Gunpowder Fall Maryland: Uses of a water resource today and tomorrow. Geological Survey Water-Supply Paper 1815.

Paul MJ, Meyer JL. 2001. Streams in the urban landscape. Annual Review of Ecology and Systematics 32: 333-365. https://doi.org/10.1146/annurev.ecolsys.32.081501.114040

PRISM Climate Group, Oregon State University, https://prism.oregonstate.edu, data created 4 Feb 2014, accessed 16 Dec 2020.

R Development Core Team. 2019. R: A language and environment for statistical computing. Vienna, Austria: R Foundation for Statistical Computing.

Rose LA, Sebestyen SD, Elliott EM, Koba K. 2015a. Drivers of atmospheric nitrate processing and export in forested catchments. Water Resources Research 51: 1333-1352. https://doi.org/10.1002/2014WR015716

Rose LA, Elliott EM, Adams MB. 2015b. Triple nitrate isotopes indicate differing nitrate source contributions to streams across a nitrogen saturation gradient. Ecosystems 18: 1209-1223. https://doi.org/10.1007/s10021-015-9891-8

Sabo, RD, Nelson, DM, Eshleman, KN. Episodic, seasonal, and annual export of atmospheric and microbial nitrate from a temperate forest. Geophysical Research Letters, 43, 2: 683-691. https://doi.org/10.1002/2015gl066758

Seto KC, Guneralp B, Hutyra LR. 2012. Global forecasts of urban expansion to 2030 and direct impacts on biodiversity and carbon pools. Proceedings of the National Academy of Sciences 109: 16083-16088. https://doi.org/10.1073/pnas.1211658109

Shuster WD, Bonta J, Thurston H, Warnemuende E, Smith DR. 2005. Impacts of impervious surface on watershed hydrology: A review. Urban Water Journal 2: 263-275. https://doi.org/10.1080/15730620500386529

Sigman DM, Casciotti KL, Andreani M, Barford C, Galanter M, Böhlke J. 2001. A bacterial method for the nitrogen isotopic analysis of nitrate in seawater and freshwater. Analytical Chemistry 73: 4145-4153. https://doi.org/10.1021/ac010088e

Sklash M, Farvolden R, Fritz P. 1976. A conceptual model of watershed response to rainfall, developed through the use of oxygen-18 as a natural tracer. Canadian Journal of Earth Sciences 13: 271-283. https://doi.org/10.1139/e76-02

Steffen W, Richardson K, Rockström J, Cornell SE, Fetzer I, Bennett EM, Biggs R, Carpenter SR, Vries Wd, Wit CAd, Folke C, Gerten D, Heinke J, Mace GM, Persson LM, Ramanathan V, Reyers B, Sörlin S. 2015. Planetary boundaries: Guiding human development on a changing planet. Science 347: 6219. https://doi.org/10.1126/science.1259855

Stevens CJ. 2019. Nitrogen in the environment. Science 363: 578-580. https://doi.org/10.1126/science.aav8215

Thompson SE, Basu NB, Lascurain Jr. J, Aubeneau A, Rao PSC. 2011. Relative dominance of hydrologic versus biogeochemical factors on solute export across impact gradients. Water Resources Research 47. https://doi.org/10.1029/2010WR009605

Tsunogai U, Komatsu DD, Ohyama T, Suzuki A, Nakagawa F, Noguchi I, Takagi K, Nomura M, Fukuzawa K, Shibata H. 2014. Quantifying the effects of clear-cutting and strip-cutting on nitrate dynamics in a forested watershed using triple oxygen isotopes as tracers. Biogeosciences 11: 5411-5424. https://doi.org/10.5194/bg-11-5411-2014

Tsunogai U, Miyauchi T, Ohyama T, Komatsu DD, Nakagawa F, Obata Y, Sato K, Ohizumi T. 2016. Accurate and precise quantification of atmospheric nitrate in streams draining land of various uses by using triple oxygen isotopes as tracers. Biogeosciences 13: 3441-3459. https://doi.org/10.5194/bg-13-3441-2016

U.S. Geological Survey, 2022, National Water Information System data available on the World Wide Web (USGS Water Data for the Nation), accessed [June 20, 2022], at URL [https://waterdata.usgs.gov/usa/nwis/uv?01589300 and https://waterdata.usgs.gov/md/nwis/uv/?site_no=01582500]

Vaughan MCH, Bowden WB, Shanley JB, Vermilyea A, Sleeper R, Gold AJ, Pradhanang SM, Inamdar SP, Levia DF, Andres AS, Birgand F, Schroth AW. 2017. High-frequency dissolved organic carbon and nitrate measurements reveal differences in storm hysteresis and loading in relation to land cover and seasonality. Water Resources Research 53: 5345-5363. https://doi.org/10.1002/2017WR020491

Walesh SG. 1989. Fundamentals of urban surface water management. Urban surface water management, p1-51. https://doi.org/10.1002/9780470172810.ch1

Walsh CJ, Fletcher TD, Ladson AR. 2009. Retention capacity: A metric to link stream ecology and storm-water management. Journal of Hydrologic Engineering 14: 399-406. https://doi.org/10.1061/(ASCE)1084-0699(2009)14:4(399)

Walsh CJ, Roy AH, Feminella JW, Cottingham PD, Groffman PM, Morgan RP. 2005. The urban stream syndrome: Current knowledge and the search for a cure. Journal of the North American Benthological Society 24: 706-723. https://doi.org/10.1899/04-028.1

Walsh J, Wuebbles D, Hayhoe K, Kossin J, Kunkel K, Stephens G, Thorne P, Vose R, Wehner M, Willis J, Anderson D, Doney S, Feely R, Hennon P, Kharin V, Knutson T, Landerer F, Lenton T, Kennedy J, Somerville R editors. 2014. Our changing climate, climate change impacts in the united states: The third national climate assessment.

Young ED, Galy A, Nagahara H. 2002. Kinetic and equilibrium mass-dependent isotope fractionation laws in nature and their geochemical and cosmochemical significance. Geochimica et Cosmochimica Acta 66: 1095-1104. https://doi.org/10.1016/S0016-7037(01)00832-8

Zhang Q, Blomquist JD, Moyer DL, Chanat JG. 2019. Estimation bias in water-quality constituent concentrations and fluxes: A synthesis for Chesapeake Bay rivers and streams. Frontiers in Ecology and Evolution 7. https://doi.org/10.3389/fevo.2019.00109

Zhang Q, Hirsch RM. 2019. River water-quality concentration and flux estimation can be improved by accounting for serial correlation through an autoregressive model. Water Resources Research 55: 9705-9723. https://doi.org/10.1029/2019WR025338

Zhang Q, Murphy RR, Tian R, Forsyth MK, Trentacoste EM, Keisman J, Tango PJ. 2018. Chesapeake Bay's water quality condition has been recovering: Insights from a multimetric indicator assessment of thirty years of tidal monitoring data. Science of the Total Environment 637-638: 1617-1625. https://doi.org/10.1016/j.scitotenv.2018.05.025

Tables

Table 1. Watershed attributes.

Water-shed	Area (ha)	Land-Use (%)				MAT (°C)	MAP (cm)	Lithology (%)		
		Forest	Agriculture	Developed	Impervious			Un-consolidated	Crystalline	Carbonate
Gwynns Falls (GWN)	8400	23.4	5.0	70.1	14.6	12.7	113.5	0	95.1	4.9
Gun-powder Falls (GUN)	41400	45.4	41.3	10.9	0.3	11.9	116.0	0	99.8	0.2

Land-use percentages were calculated from the 2016 National Land Cover Database, impervious is the sum of medium and high intensity developed land-use classes; agricultural land represents the sum of both cultivated crop and pasture/hay land classes (Homer et al., 2020). Land use percentages do not sum to 100% as all land use classes are not listed (e.g. open water, wetlands). MAT = Mean Annual Temperature, MAP = Mean Annual Precipitation. Note that MAT and MAP cover the time period from 1981-2010 (PRISM, 2014). Lithology data were obtained from Zhang et al. 2019.

Figures

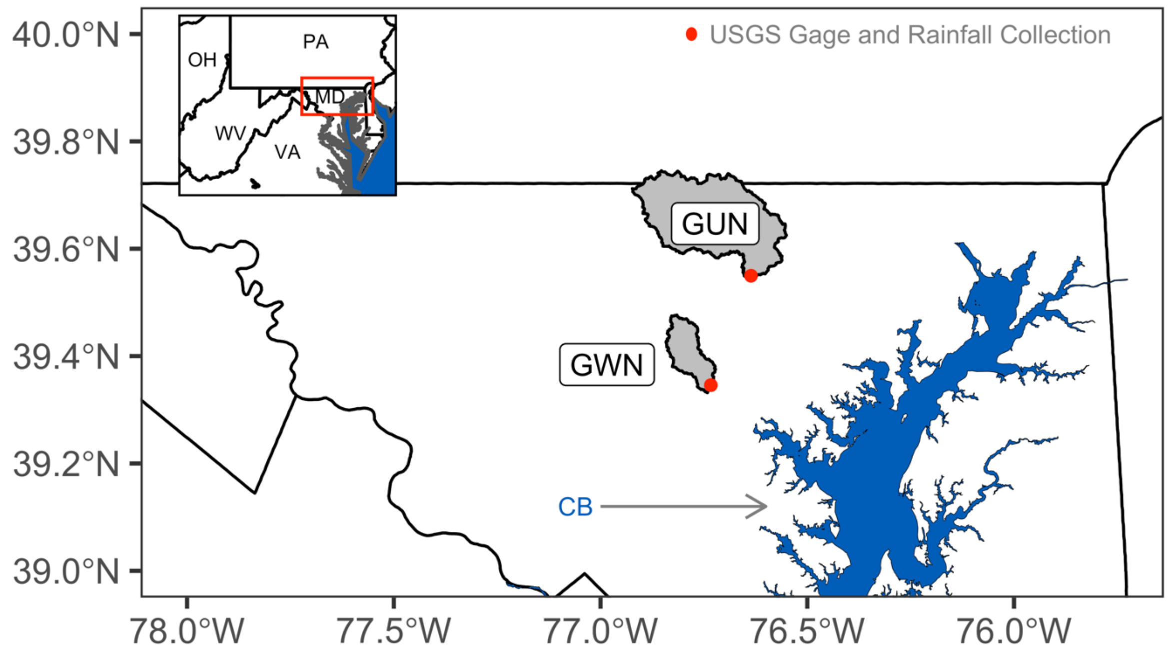

Figure 1. Site map showing watershed boundaries (GWN = Gwynns Falls, GUN = Gunpowder Falls), United States Geology Survey (USGS) gaging stations and rainfall collection sites, and Chesapeake Bay (CB) location. Inset map shows relative position of watersheds in Maryland (MD) relative to neighboring states (PA = Pennsylvania, OH = Ohio, WV = West Virginia, VA = Virginia).

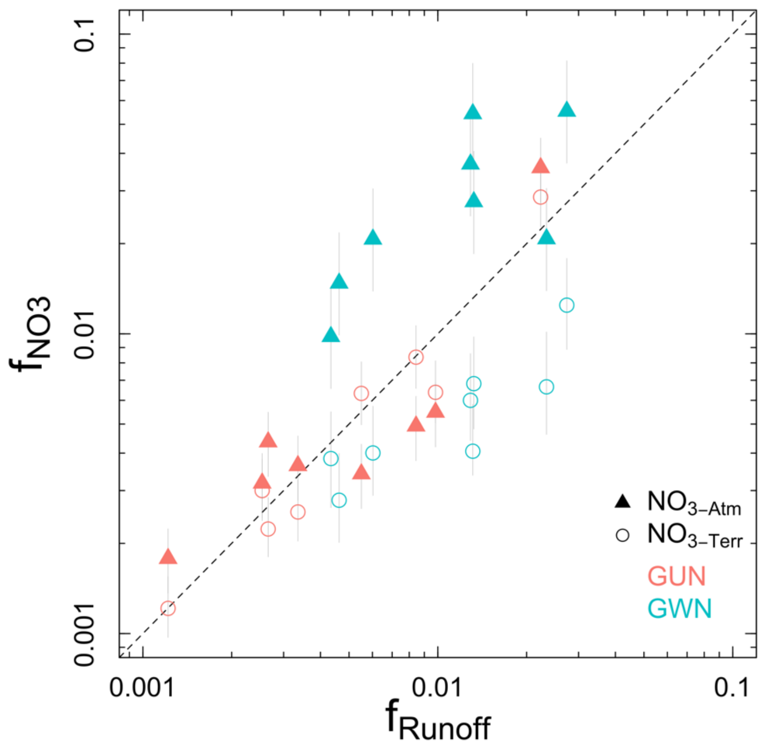

Figure 2. Fraction of NO_3^- loads (fNO3; separated by NO_3^-Terr, circles, and NO_3^-Atm, triangles) and discharge (fRunoff) during the study duration (14 months) represented by sampled storm events (n = 8). Points falling above the dashed line (1:1 line) indicate storm events have an outsized impact on NO_3^- loads and points falling below the line indicate baseflow has an outsized impact on NO_3^- loads. Points on or near the 1:1 line indicate a chemostatic response, in which storms nor baseflow have an outsized impact on NO_3^- loads.

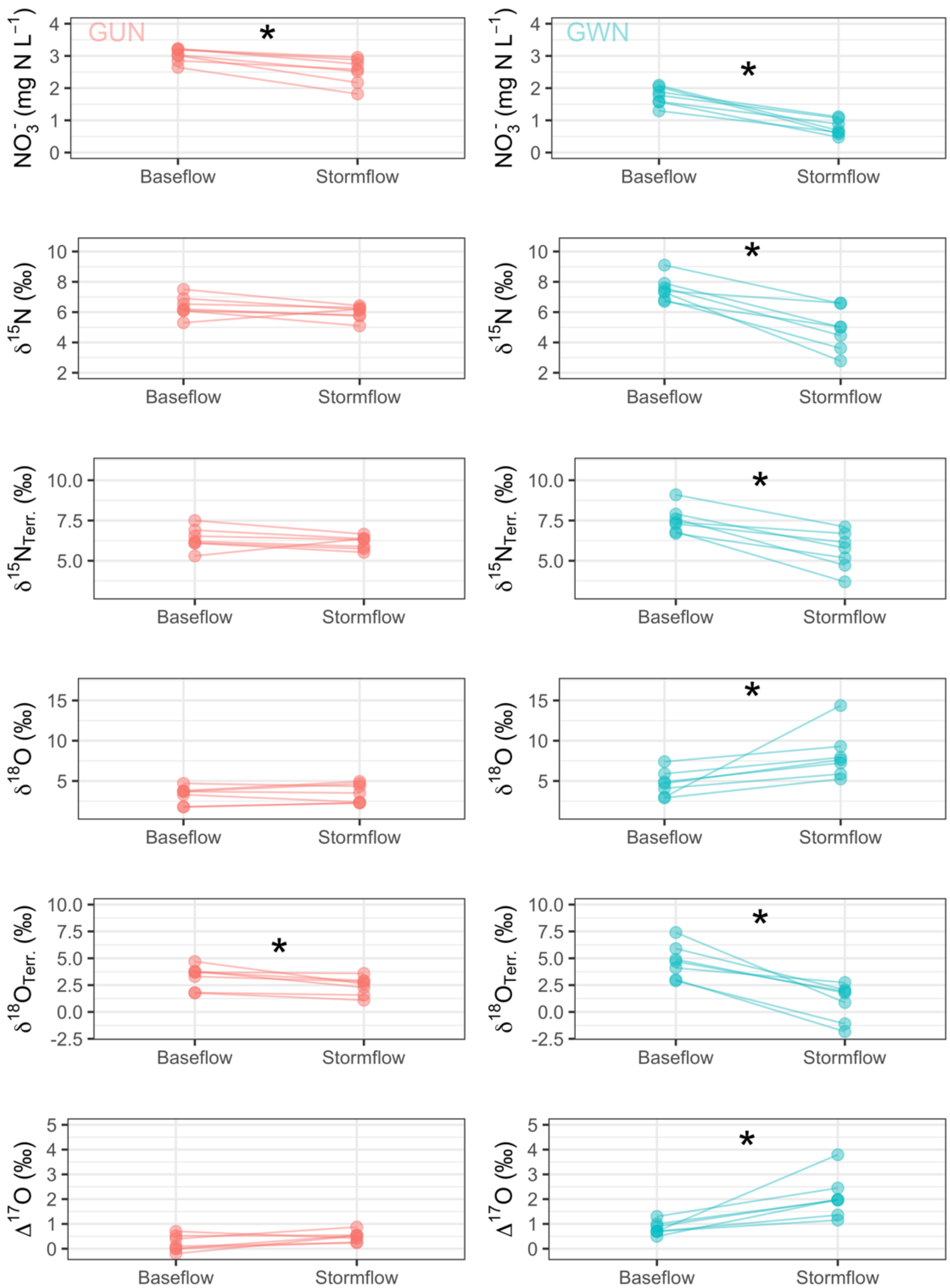

Figure 3. Event mean NO_3^- concentrations and $\delta^{15}N$, $\delta^{15}N_{Terr}$, $\delta_{18}O$, $\delta^{18}O_{Terr}$, and $\Delta^{17}O$ values of NO_3^- for samples collected during storm events paired with the corresponding baseflow sample preceding the event. Asterisk (*) indicates significant difference at $p < 0.05$ as determined using a Wilcoxon ranked-sum test.

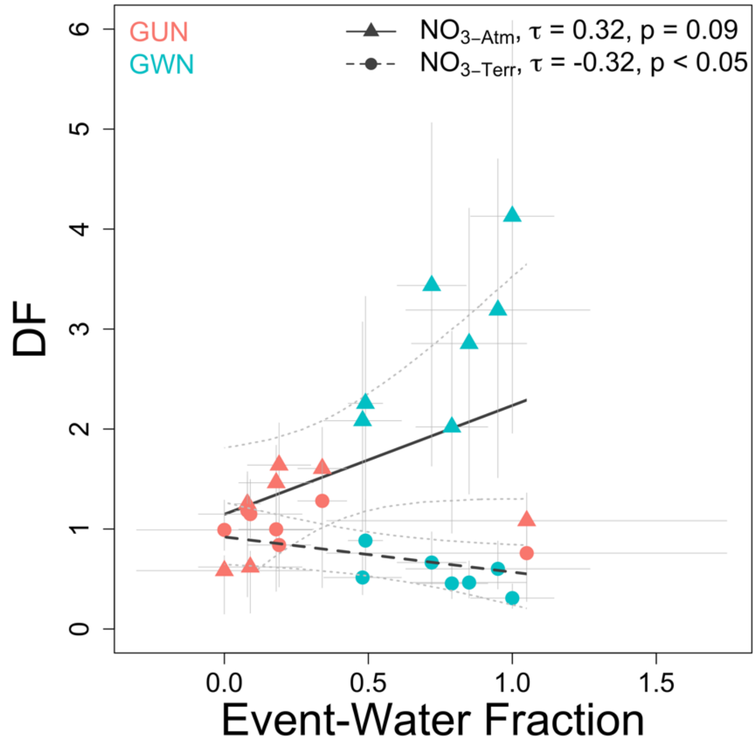

Figure 4. Disproportionality factor (DF) and event-water fraction for $NO_3^-{}_{Atm}$ (triangles) and $NO_3^-{}_{Terr}$ (circles). Event-water fraction and DF are positively, but not significantly correlated for $NO_3^-{}_{Atm}$ ($\tau = 0.32$, $p = 0.09$) while event-water fraction and DF are significantly, negative correlated for $NO_3^-{}_{Terr}$ ($\tau = -0.32$, $p < 0.05$) across both watersheds. The thin, dotted line shows bootstrapped 95% confidence intervals.

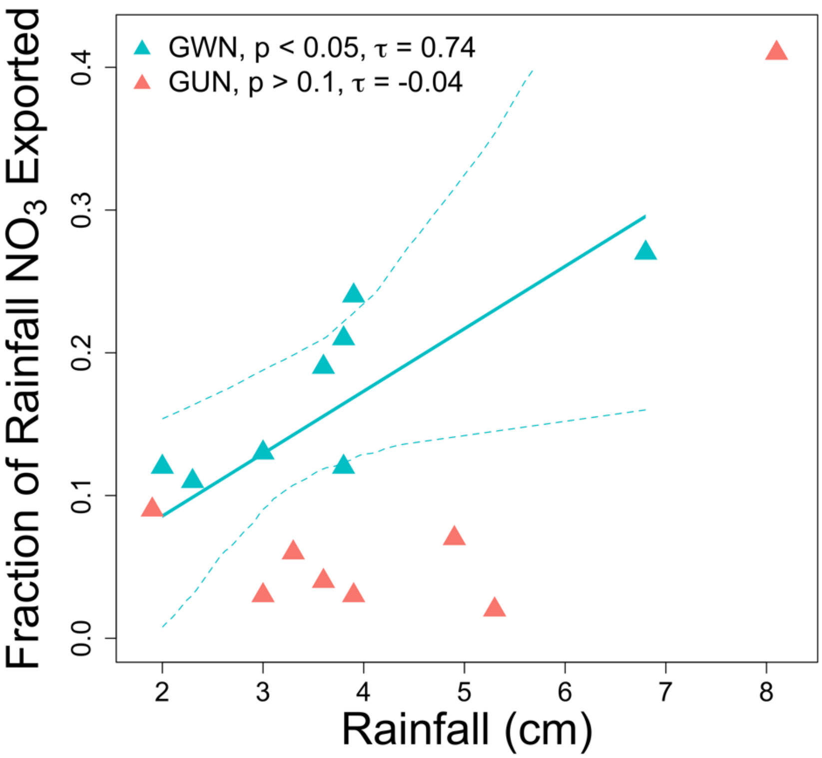

Figure 5. The fraction of NO_3^- in rainfall that is exported in streamwater during the same event is positively significantly related with total event rainfall at GWN ($p < 0.05$, $\tau = 0.74$) but not at GUN ($p > 0.1$, $\tau = -0.04$). The solid line is the Theil-Sen slope and the thin, dotted line shows the bootstrapped 95% confidence intervals.

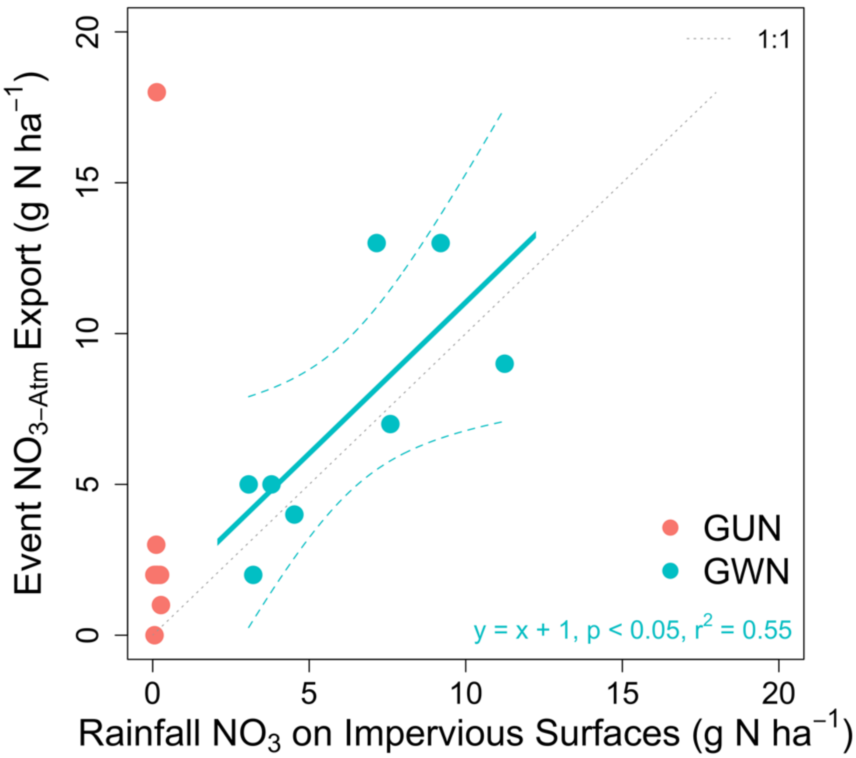

Figure 6. The event $NO_3^-{}_{Atm}$ yield (in g N ha^{-1}) has a 1:1 relationship with the estimated rainfall $NO_3^-{}_{Atm}$ deposition on impervious surfaces (in g N ha^{-1}) at GWN (slope = 1.00, intercept = 1, r^2 = 0.55, $p < 0.05$), but not at GUN.